

Coffee bean particle motion in a spouted bed measured using Positron Emission Particle Tracking (PEPT)

Al-Shemmeri, Mark; Windows-Yule, Christopher; Lopez-Quiroga, Estefania; Fryer, Peter

DOI:

[10.1016/j.jfoodeng.2021.110709](https://doi.org/10.1016/j.jfoodeng.2021.110709)

License:

Creative Commons: Attribution-NonCommercial-NoDerivs (CC BY-NC-ND)

Document Version

Peer reviewed version

Citation for published version (Harvard):

Al-Shemmeri, M, Windows-Yule, C, Lopez-Quiroga, E & Fryer, P 2021, 'Coffee bean particle motion in a spouted bed measured using Positron Emission Particle Tracking (PEPT)', *Journal of Food Engineering*, vol. 311, 110709. <https://doi.org/10.1016/j.jfoodeng.2021.110709>

[Link to publication on Research at Birmingham portal](#)

General rights

Unless a licence is specified above, all rights (including copyright and moral rights) in this document are retained by the authors and/or the copyright holders. The express permission of the copyright holder must be obtained for any use of this material other than for purposes permitted by law.

- Users may freely distribute the URL that is used to identify this publication.
- Users may download and/or print one copy of the publication from the University of Birmingham research portal for the purpose of private study or non-commercial research.
- User may use extracts from the document in line with the concept of 'fair dealing' under the Copyright, Designs and Patents Act 1988 (?)
- Users may not further distribute the material nor use it for the purposes of commercial gain.

Where a licence is displayed above, please note the terms and conditions of the licence govern your use of this document.

When citing, please reference the published version.

Take down policy

While the University of Birmingham exercises care and attention in making items available there are rare occasions when an item has been uploaded in error or has been deemed to be commercially or otherwise sensitive.

If you believe that this is the case for this document, please contact UBIRA@lists.bham.ac.uk providing details and we will remove access to the work immediately and investigate.

1 **Coffee bean particle motion in a spouted bed measured using Positron Emission**

2 **Particle Tracking (PEPT)**

3

4 **Mark Al-Shemmeri**

5 Email: mxa118@student.bham.ac.uk

6 School of Chemical Engineering

7 University of Birmingham

8 Birmingham B15 2TT, UK

9

10 **Kit Windows-Yule**

11 Email: c.r.windows-yule@bham.ac.uk

12 School of Chemical Engineering

13 University of Birmingham

14 Birmingham B15 2TT, UK

15

16 **Estefania Lopez-Quiroga**

17 Email: e.lopez-quiroya@bham.ac.uk

18 School of Chemical Engineering

19 University of Birmingham

20 Birmingham B15 2TT, UK

21

22 **Peter J. Fryer***

23 *Corresponding author

24 Email: p.j.fryer@bham.ac.uk

25 School of Chemical Engineering

26 University of Birmingham

27 Birmingham B15 2TT, UK

28 **Coffee bean particle motion in a spouted bed measured using Positron Emission**
29 **Particle Tracking (PEPT)**

30 Mark Al-Shemmeri^{1,2}, Kit Windows-Yule¹, Estefania Lopez-Quiroga¹, Peter J. Fryer^{1*}

31 ¹ School of Chemical Engineering, University of Birmingham, B15 2TT, UK.

32 ² Jacobs Douwe Egberts, R&D Offices, OX16 2QU, UK.

33

34 **Abstract**

35 Coffee roasting is a heat treatment process that transforms green coffee into a product that can
36 subsequently be ground and brewed. Understanding roasting is critical in developing new
37 downstream processes and formulations, as well as in optimising existing ones. Positron
38 Emission Particle Tracking (PEPT) allows tracking of particles in process equipment and has been
39 used here to characterise particle dynamics of coffee beans within a spouted bed roaster subject
40 to varying air-to-bean ratios without roasting. Occupancy profiles associated with each air-to-bean
41 ratio have been determined and two distinct regions identified: (i) a *dense* bean bed of high
42 occupancy (ii) a *dilute* freeboard of lower occupancy. Results also revealed the effect of coffee
43 density on particle dynamics within the roaster. Overall, this work demonstrates that PEPT can
44 be a useful tool to generate data regarding granular flow patterns in roasters that might be used
45 to improve existing heat and mass transfer models for roasting.

46

47 **Keywords:** Positron Emission Particle Tracking (PEPT); spouted bed of coffee beans; particle
48 motion modelling; air-to-bean ratio; coffee roasting degree and density

49

50 **1 Introduction**

51 Coffee roasting is a heat treatment process that transforms green coffee via changes in hydration,
52 chemical composition and microstructure. During roasting, coffee is subject to high temperature
53 air flows, applied via specific time-temperature roasting profiles, so moisture content decreases
54 in an endothermic drying process (Alessandrini et al., 2008; Pittia et al., 2011; Romani et al.,
55 2012; Schenker, 2000). These time-temperature profiles are designed based on empirical
56 evidence, trial and error, or simply the experience of the roast master. Manipulations of
57 temperature, air flow, batch size and roast time all influence the roasting profile; the ability to
58 manipulate these parameters allows the coffee's characteristic flavour and aroma to be developed
59 (Hoos, 2015; Rao, 2020) – complexity of profile manipulation has been discussed in detail by
60 Hoos (2015); Rao (2014, 2020).

61 Once the free moisture has been removed in the early stages of roasting the colour of the coffee
62 gradually changes from pale green to yellow (Geiger et al., 2005; Rao, 2014; Schenker, 2000;
63 Wang and Lim, 2012). As the coffee temperature increases beyond 170°C-190°C, the initially
64 endothermic roasting process becomes exothermic, with the beginning of Maillard reactions,
65 causing the colour to shift from yellow to brown (Schenker, 2000). The combined effect of heat
66 generation in the bean's core – leading to water vapour within the bean – and the formation of
67 CO₂, increases the internal pressure until the bean's structure fails, releasing an audible “crack”
68 that coincides with a significant expansion in both volume and surface area (Geiger et al., 2005;
69 Rao, 2014; Schenker, 2000; Wilson, 2014). The period after this *‘first crack’*, described in specialty
70 coffee as the *development time*, has been highlighted as being critical to control due to rapid
71 changes in physicochemical properties (Hoos, 2015). Beyond first crack, oils migrate to the
72 coffee's surface and carbon dioxide accumulates until *second crack* occurs (Rao, 2014; Wilson,
73 2014; Yergenson and Aston, 2020).

74 Once the desired end-point of the roast has been reached the coffee is cooled by either cool air
75 or quench water (Baggenstoss et al., 2008; Schenker, 2000).

76 The physicochemical transformations that occur during roasting are numerous and inter-related.
77 Monitoring changes in physical and chemical properties of coffee during roasting is critical as
78 rapid transformations in colour, volume and density occur through both first crack and
79 *development time* (Alessandrini et al., 2008; Bustos-Vanegas et al., 2018; Garcia, et al., 2018;
80 Yergenson and Aston, 2020). The commercial need is to understand and predict how to control
81 the roast to improve product quality and process efficiency. This can be achieved either using
82 empirical correlations, or through physics-based predictive models.

83 Particle and fluid interactions govern heat and mass transfer (Bergman et al., 2011), yet little work
84 has been done to characterise coffee roasting. Whilst both air flow and batch size are critical to
85 coffee development and roasting (Kwak et al., 2017), there is little literature on their effect on
86 coffee during roasting aside from those documented by Rao (2014, 2020). Cristo et al. (2006) and
87 Resende et al. (2017) used photography in transparent drums to visualise dynamic behaviour of
88 coffee in rotating drums.

89 Computational Fluid Dynamics (CFD) can be used to model and predict flow behaviour in *dilute*
90 granular systems (Abdul Ghani et al., 2019; Alonso-Torres et al., 2013; Chiang et al., 2017;
91 Oliveros et al., 2017). Coupled CFD and Discrete Element Method (DEM) can simulate lumped
92 and distributed temperature distributions within spouted bed roasters (Azmir et al., 2020;
93 Bruchmüller et al., 2010) but is often difficult to validate. Bruchmüller et al. (2010) established a
94 DEM model to describe the development of temperature and moisture within a fluidised bed of
95 spherical particles during roasting. This enabled single-bean resolution of temperature and
96 moisture distributions within the batch, founded on fundamental physical phenomena. Azmir et
97 al. (2020) studied a similar system at lower temperatures (50-200°C) incorporating particle
98 shrinkage – effects of initial moisture content, density and particle size were highlighted.

99 PEPT is a non-invasive technique that can characterise flow behaviour within granular systems.
100 The trajectories of particles labelled with positron-emitting radioisotopes can be tracked in three-
101 dimensions with high temporal and spatial resolution (Windows-Yule et al., 2020). The principles
102 of PEPT are described in detail by Parker et al. (1993) and Parker (2017), while PEPT's best
103 practices and applications were recently reviewed by Windows-Yule et al. (2020). PEPT
104 measurements are typically performed on steady-state systems in real process equipment
105 (Windows-Yule et al. 2020) and thus experimental design includes part-processed products to
106 emulate the changes in material properties that occur during operation. Characterisation of
107 particle dynamics could give the ability to fundamentally describe heat and mass transfer
108 independent of roaster design. For industry, the need is to transform development and innovation
109 of both roasting process and product into an off-line exercise.

110 Here, PEPT has been used to study the particle dynamics of coffee in a pilot-scale spouted bed
111 roaster that is representative of full-scale systems, with the aims of (i) understanding the granular
112 flow patterns in the roaster and (ii) showing that the resulting data provides boundary conditions
113 that might be integrated within a suitable thermal model to predict time-temperature profiles during
114 roasting. The experimental design was selected to emulate changes during roasting. As PEPT
115 measurements require long data capture times, and high temperature roasting incurs rapid
116 transformation of the coffee's physicochemical properties, PEPT measurements of real roasting
117 are not possible. By studying coffees of different roast degrees and densities (thus emulating the
118 changes in physicochemical properties during roasting), the corresponding particle dynamics at
119 different stages of real roasting can be inferred.

120 **2 Materials & Methods**

121 2.1 Coffee beans

122 Before PEPT measurements, batches of 350g of Kenyan Arabica coffee were isothermally
123 roasted in a spouted bed roaster (RFB-S, Neuhaus Neotec) at a temperature of 250°C and a fan
124 frequency of 48 Hz (i.e., inlet air velocity of 7.2 m s⁻¹). Part-roasted and roasted samples were
125 obtained by roasting for 2 mins 18 s (138 s) and 4 mins 38 s (278 s), respectively; green coffee
126 samples were not roasted. Coffee samples from triplicate roasts were combined and well mixed
127 prior to PEPT studies to minimise variations between batches.

128 Intrinsic density was determined by measuring the coffee bean's principal dimensions (digital
129 calipers, IP54, Perciva) and mass (XSR204, Mettler-Toledo); 25 beans from each sample set
130 were measured. From the bean dimensions, *a* (width), *b* (depth) & *c* (length) (*mm*), bean volume,
131 V_b (*mm*³) was calculated assuming bean geometry is that of a hemi-ellipsoid ($V_b \approx \frac{\pi abc}{6}$). Bulk
132 density was calculated from the measured mass (Lunar balance, Acaia) of coffee that occupies a
133 250 ml beaker, where beans settled freely. The top of the beaker was smoothed to ensure a level
134 fill and measurements were repeated in triplicate using aliquots of each sample set. Coffee
135 properties are presented in Table 1.

136 2.2 Coffee roaster

137 The same spouted bed roaster that produced the roasted coffee samples was used here for flow
138 studies. A simplified schematic of the roasting chamber is presented in Figure 1 (a). To support
139 the description of the system volume, Figure 1 (b) highlights the orientation of the roaster within
140 the space between gamma-ray detector heads. The centre of the roasting chamber was used as
141 the origin for the data.

142 Both the velocity and mass flow rate of air inputs to the roaster were determined as a function of
143 the fan frequency using a hot-wire anemometer (405i, Testo) installed on the inlet air pipe (ø 60
144 mm) between the blower and heating element. The roaster was operated at ambient temperature
145 (c. 25°C) with fan frequencies of 30-60 Hz at 5 Hz intervals for 10 mins. An average velocity for

146 each fan frequency was calculated and used to determine inlet air mass flow rates. Table 2
147 outlines the corresponding air velocities and mass flow rates for several fan frequency set points.

148 *2.2.1 Roaster fill volume*

149 The volume occupied by a static bean bed (i.e., coffee beans within the roasting chamber with no
150 applied heat, or airflow) was determined using the coffee's bulk density, specified batch size and
151 roaster geometry. The bean bed was assumed uniform along the *z direction*, according to Figure
152 1 (b), with a depth of 9.8 cm. The equivalent area occupied by a static bed of beans in the plane
153 *xy* of the roaster, according to Figure 1 (b), is thus a function of the coffee's batch size and bulk
154 density, in addition to the geometry and depth of the roaster. Table 3 outlines the static bean bed
155 area according to batch size and coffee density.

156 2.3 Positron Emission Particle Tracking (PEPT)

157 *2.3.1 Experimental setup & tracer labelling*

158 The spouted bed roaster was placed between two detector heads of a modified ADAC Forte
159 positron camera, such that the roasting chamber falls at the centre of the camera's most sensitive
160 region, parallel to the detector heads - ensuring both a maximal acquisition rate and precision.
161 Further details of the positron camera are given in Parker et al. (2002) and Windows-Yule et al.,
162 (2020).

163 A single coffee bean was selected from each sample set; principal dimensions of the selected
164 particles were checked to be within one standard deviation of the batch's mean. Selected particles
165 were indirectly labelled by pipetting 2 ml of water – containing ions of Fluorine-18, a β^+ -emitting
166 radioisotope - onto the particle's surface (Parker, 2017). After allowing 15 mins for absorption of
167 irradiated water, excess water, determined gravimetrically, was removed by drying the coffee
168 bean under a heat lamp. A balance with 0.1 mg precision (XSR204, Mettler-Toledo) was used to
169 measure the mass before and after labelling, ensuring that the two agreed to within the stated

170 precision of the balance. The labelled coffee bean was returned to the sample set and placed in
171 the roaster.

172 All experiments were conducted in accordance with the Positron Imaging Centre's Local Rules,
173 under the supervision of a trained radiation protection supervisor.

174 *2.3.2 Experimental procedure*

175 The experimental design intends to emulate roasting through the study of coffee beans of different
176 roast degrees and densities and reflects realistic variations of air-to-bean ratio that a roaster might
177 employ. Air-to-bean ratio is defined as the ratio of the total mass of air input to the roaster during
178 a roast (i.e., the product of the mean air mass flow rate and total roast time) to the mass of the
179 batch. The experimental conditions considered a range of batch sizes (200, 350 and 500 g), air
180 flows (fan frequencies of 30, 39, 48 and 65 Hz) and roast degrees (green, part-roasted and
181 roasted). Minimum airflow for spouting of 350 and 500 g batches of green coffee corresponded
182 to fan frequencies of 39 and 48 Hz, respectively. As spouting is required for roasting conditions
183 to be safely employed in a commercial setting, only fan frequencies of 48 and 65 Hz were studied
184 for 500g batch sizes; fan frequencies of 39, 48 and 65 Hz were studied for 350g batches and 30,
185 48 and 65 Hz for 200g batches.

186 For the system to be considered ergodic, data was captured over a period sufficient for the tracer
187 particle to fully explore the roasting chamber. Thus, once particle motion was established at
188 ambient temperatures (c. 25°C), data was captured for 60 mins.

189 *2.3.3 Time average analysis of cartesian co-ordinates*

190 For steady-state systems, it is assumed that the time averaged behaviour exhibited by a single
191 particle in a homogenous system is representative of the ensemble-averaged behaviour of all
192 particles in the system (Wildman et al., 2000). From this, the system can be considered ergodic
193 and therefore it is expected that the fractional residence time of the tracer in any given region, is

194 directly proportional to the typical fraction of total particles in that region at any given point in time
195 (Windows-Yule et al., 2020).

196 Experimental datasets – containing Cartesian coordinates at time intervals of 0.01-0.1
197 milliseconds (dependent on tracer activity) – were segmented to account for systemic variability
198 such that each 60 min experiment generated three 20 mins datasets. These time-segmented
199 datasets were subsequently analysed in MATLAB (2020a, MathWorks). For analysis of ergodic
200 systems, with the allowance of sufficient time for data capture and appropriate sizing of mesh
201 element dimensions, the decay of the tracer's activity, with a half-life of 109 mins, is assumed to
202 have no significant impact on the resultant time-segmented occupancy profiles.

203 *2.3.4 Occupancy profiles*

204 Occupancy of the system is determined by division of the system's volume into uniform elements
205 (pixels in 2D, voxels in 3D). Here, a system of 100x100 elements in 2D was established as
206 depicted in Figure 2 (a), where mesh element dimensions were approx. equivalent to the camera's
207 intrinsic spatial resolution. For a tracer moving at 7 m s^{-1} (equal to the mean inlet air velocity of
208 the roaster) the tracer can be located within approx. 3.5mm (Parker et al., 2002), so mesh element
209 dimensions of 3.5x3.5 mm in 2D were used. Occupancy profiles shown in Figure 2 (b) – where
210 high occupancy regions are red; low occupancy regions are dark blue – are expressed as a
211 fraction of total experimental time and are determined knowing the residence time of the tracer in
212 each element; the occupancy within each element is proportional to the mean packing density of
213 particles (Windows-Yule et al., 2020).

214 *2.3.5 Delineation and resolution of occupancy profiles*

215 The occupancy profiles in Figure 2 (b) reveal the existence of two different regions: a *dilute* (i.e.,
216 low occupancy) freeboard and a *dense* (i.e., high occupancy) bean bed. The sum of these two
217 regions is defined here as the area of the roaster in a given two-dimensional plane (A_o) that is

218 occupied under the specified roasting conditions, and it is determined from the number of non-
219 zero elements in a given two-dimensional plane (n_{nze}) and the elemental area (A_e) of occupancy
220 profiles (Figure 2 (b)) as follows:

$$A_o = \sum n_{nze} A_e \quad \text{Eq. (1)}$$

221 The bean bed area is determined via application of an Otsu method (Otsu, 1979) to normalised
222 probability distributions of one-dimensional (in y) occupancy profiles – implemented in MATLAB
223 (2020a, MathWorks). Threshold values were determined for each occupancy profile - as
224 illustrated in Figure 3 - as the value is dependent on the distribution of fractional residence times
225 observed for each occupancy profile. It is assumed that occupancies below the threshold value
226 are associated with the *dilute* freeboard, while occupancies over that threshold value relate to the
227 *dense* bean bed. The area occupied by the bean bed (A_b) is calculated using a similar approach
228 to that used to calculate the overall occupied area (i.e., Eq. (1)).

229 2.3.6 Particle trajectories, residence times and spatial velocity distributions

230 Spatial velocity distributions are used here to identify granular flow patterns in the *dilute* freeboard
231 and *dense* bean bed. Both the velocity and time spent by a particle in each region (i.e., residence
232 time), can be determined using the individual particle trajectories – Figure 2 (c) shows consecutive
233 particle trajectories defined using the bed's location. Beans crossing the bean bed-spout interface
234 twice in rapid succession caused a large number of low residence times, so individual particle
235 trajectories corresponding to residence times below 0.01% of maximum residence time in each
236 region for a specified condition were omitted. Particle velocities were then determined as
237 described by Windows-Yule et al. (2020).

238 3 Results

239 During roasting, bean properties vary significantly. To study these changes and the effects they
240 have on coffee bean particle motion, experiments were conducted at ambient temperatures where

241 the roaster was filled with green, part-roasted and fully-roasted beans (prepared prior to PEPT
242 measurements as discussed above). The data sets thus show the changes in behaviour that will
243 occur during roasting.

244 3.1 Occupancy and velocity profiles in the roaster

245 Both occupancy and velocity profiles have been obtained from PEPT data as explained in Section
246 2 for different bean densities (i.e., green, part-roasted and roasted), air flow frequencies (i.e.,
247 velocities) and batch sizes, and are presented next. Overall, these results define two different
248 occupancy regions (i) a *bed* of high solids fractions through which beans move slowly (<0.5 m s-
249 1) together with (ii) a spout of beans – the *freeboard* – moving rapidly (0.5-1.5 m s-1) upwards at
250 the air inlet which then fall to the surface of the bed.

251 3.1.1 Effect of bean density

252 Figure 4 shows PEPT data for 350g batches of green, part-roasted and roasted coffee at a
253 constant fan frequency of 48 Hz, thus indicating how particle (i.e., bean) motion in the roaster
254 changes as a function of bean density – during a real roast, the density of the beans would change
255 reflecting that of the studied green, part-roasted and roasted beans. Occupancy plots, i.e., Figure
256 4 (a)-(c), show low occupancy values for the upper part of the roaster (the freeboard), while
257 occupancy at the bottom of the chamber decreases with bean density. For example, green beans,
258 with higher bean density, tend to occupy the bottom region of the roaster, forming a small bed of
259 high occupancy (red region in Figure 4 (a)). Fully roasted beans, with lower bean density, form
260 larger beds, but less densely occupied (green region in Figure 4 (c)) – lower density makes beans
261 easier to fluidise and spout.

262 Velocity profiles presented in Figure 4 (d)-(f) reveal that there is a general rotation of the beans
263 around a point within the bed near the spout region (most evident in Figure 4 (c)), with the highest
264 bean velocities corresponding to the rise and fall of beans in the spouted bed freeboard.

265 3.1.2 *Effect of air flow*

266 Figure 5 shows PEPT data for 200g batches of green coffee at different fan frequencies, thus
267 showing how bean motion changes with airflow. As air flow increases, the total area occupied by
268 coffee in the roaster significantly increases (see Figure 5 (a)-(c)), as higher air flows ease
269 fluidisation. The corresponding velocity profiles (see Figure 5 (d)-(f)) also show an increase of
270 bean velocity in the freeboard with increasing airflow; the high occupancy region (i.e., the bed) is
271 again slow moving. Figure 5 (f) shows the rotational nature of the flow most clearly. At this highest
272 airflow, a new, circulating flow regime with no true bean bed was established (Figure 5 (c)). This
273 shows in the reduced red region of high occupancy (see Figure 5 (c)) and the corresponding
274 velocity profile (see Figure 5 (f)), which shows the rotation of beans around a point closer to the
275 spout. This phenomenon is unique to these conditions due to the combination of a high coffee
276 density and high air-to-bean ratio - smallest batch and highest fan frequency.

277 3.1.3 *Effect of batch size*

278 Figure 6 shows PEPT data for 200, 350 and 500g batches of roasted coffee at a fan frequency of
279 48 Hz, thus showing how beans motion changes with batch size. For these conditions, the region
280 with the higher occupancy levels – red area at the bottom of the roaster in Figure 6 (a) - becomes
281 larger and less dense as batch size increase - see Figure 6 (b)-(c). Bean velocities associated to
282 these bed regions are the slowest within each of the systems, as shown in Figure 6 (d)-(f).

283 For larger batches of roasted coffee (see Figure 6 (c)), two occupancy bands are visible in the
284 bean bed. The larger band in the centre of the bean bed (see Figure 7 (b)), corresponds to beans
285 that follow the modal freeboard trajectory, from the spout into the bed - shown by the densely
286 populated particle trajectories in the top part of the roasting chamber (visible in Figure 7(a)) - and
287 fall downward to the spout, parallel to the wall. The smaller band is formed at the top of the bean

288 bed, near the spout, and is caused by beans that are propelled with less force, leading to scattered
289 motion in this region, as shown in Figure 7 (b).

290 *3.1.4 Combined effect of coffee density, air flow and batch size on roaster occupancy*

291 Figure 8 (a)-(c) plots the variation of total occupied area of the roasting chamber for all
292 experimental conditions obtained from PEPT data - note that bulk density decreases with a higher
293 roasting degree (see Table 1). The occupied area of all batch sizes tends toward the capacity of
294 the roasting chamber as airflow increases. For low air-to-bean ratios (i.e., large batch size and
295 low airflow), the maximum area is achieved at lower airflow (Figure 8 (a)-(c)) due to the greater
296 fill volumes (i.e., larger occupied areas in plane xy) for larger batch sizes. Occupied area at high
297 airflow (65 Hz) decreases with batch size and increases as coffee density decreases. For
298 moderate airflow (48 Hz), occupied area increases as coffee density decreases, yet occupied
299 areas of part-roasted and roasted coffee systems are not significantly different, thus the impact
300 of batch size is not significant for part-roasted and roasted coffee.

301 Figure 8 (d)-(f) plots the variation in bed area for all experimental conditions. Lower density coffees
302 (i.e., roasted beans that have lost mass, but increased in size) are more easily spouted than the
303 higher density (green) coffee, and thus bean bed mass decreases with density, however bed area
304 increases with decreasing density due to volumetric expansion (see Table 2). For all conditions,
305 bed area increases with batch size; for a given batch size, while increasing airflow decreases the
306 bed area, the effect is less significant than the change in density.

307 *3.1.5 Residence time*

308 Figure 9 presents cumulative distributions of residence time that result from changes in coffee
309 density, airflow and batch size. The data is presented as the residence times in the bean bed, the
310 freeboard, and recirculation times (from spout-to-spout); residence times in the bean bed and
311 freeboard were identified as shown in Figure 7.

312 Figure 9 (a) shows that as coffee density decreases, residence times in the bed increase, while
313 freeboard residence times decrease slightly. As coffee bean density decreases, beans are more
314 easily fluidised, and have faster freeboard velocities leading to smaller residence times (Figure 9
315 (b); also seen in Figures (4)-(6)).

316 Figure 9(d-f) shows bean bed residence times increase at lower airflows; they also indicate that,
317 for roasted coffee, the variation in residence time (as seen in Figure 7 (a)) decreases with airflow.
318 Spout-to-spout recirculation times presented in Figure 9 (b) are mostly affected by bean bed travel
319 as particle velocities in the freeboard are much greater than in the bed for all bean densities.

320 Under moderate airflow (48 Hz), Figure 9 (g) reveals that the larger the batch size, the greater
321 the bean bed residence time: greater fill volumes (i.e., larger bed areas in plane xy , as shown in
322 Figure 6) result in longer bean bed travel distances from the surface to the spout. For moderate
323 airflows (48 Hz), batch sizes of 500 and 200g roasted coffee correspond to bed heights of 17.5
324 and 11.9 cm, respectively. As bed height increases with fill volume, the downward freeboard travel
325 distance decreases, thus in the freeboard, larger batch sizes are associated with shorter
326 residence times.

327 3.2 Bean dispersion

328 The occupied area of coffee in the roasting chamber is defined by the dispersion of the beans
329 propelled from the spout, i.e., the variation between individual freeboard trajectories, such as
330 those shown in Figure 7 (a) (Windows-Yule et al., 2020). The distribution of the vertical component
331 for coffees of different densities in a 200g batch at moderate airflow (48 Hz), is presented in Figure
332 10 (a), and that for the horizontal component is shown in Figure 10 (b). It can be seen that (i) for
333 green coffee, there is very little vertical distance travelled, reflecting the low fluidisation of high-
334 density particles, whilst there is much greater vertical displacement of the roasted, and thus

335 lighter, coffees, (ii) the horizontal distance travelled by beans increases as the coffee density
336 decreases.

337 **4 Implications for Heat Transfer**

338 4.1 Regional variation of heat transfer

339 Bean bed and freeboard heat transfer behaviour will be different due to the different flow patterns
340 in each region that have been revealed in this work:

341 (i) Freeboard region. The heat transfer coefficient in the spout will be high as the beans will be
342 subject to significant air-to-bean convective heat transfer. The coffee temperature will also
343 increase rapidly through contact with the hottest air.

344 (ii) Bean bed region. Within the bed, heat transfer is governed by a number of mechanisms,
345 including: bean internal conduction, bean-to-bean surface conduction (contact), bean-to-bean
346 surface radiation (non-contact), air-to-bean convection, convection in voids, and the effective
347 thermal conductivity of the bed (Díaz-Heras et al., 2020).

348 These two regions will present very different heat transfer mechanisms and depending on the
349 intended product, both present positive and negative impacts on potential cup quality. A thermal
350 model for roasting will combine the particle motion data's residence times in both regions with
351 thermal boundary conditions appropriate to each; beans that flow from spout-to-spout - through
352 the roaster - will experience a range of conditions.

353 As the temperature difference between bean and air decreases, so will heat transfer (Brown and
354 Lattimer, 2013). In the bed, the region adjacent to the spout will likely be at a higher temperature
355 than the centre of the bed. The temperature of the metal will be close to that of the adjacent
356 beans.

357 The increase in total occupied area during roasting, and thus increased fraction of beans in the
358 freeboard, indicates that a greater fraction of beans will be subject to convective heat transfer in
359 the latter stages of roasting. Cheng et al. (2020) found that heat conduction through bed voids
360 increases with bed porosity and is significant for systems where the air to particle conductivity
361 ratio is less than 5, as it is here. Therefore, as bed fluidisation and porosity increases, conductive
362 heat transfer through the voids can be expected to increase, improving bed heat transfer.

363 4.2 Heat transfer efficiency

364 Although increasing heat transfer rates is desirable to improve productivity (due to shorter process
365 times) and yield (as a faster roast typically has a lower mass loss), the impact on flavour is a
366 concern - faster roasts tend to provide underdeveloped coffees. For commercial roasting it may
367 be best to start with moderate air flow, and to reduce it as coffee density changes to maintain a
368 consistent occupancy profile. Reduction of air flow during roasting also acts to suppress exothermic
369 reactions that are initiated around first crack (Schwartzberg 2002) – seen in a sudden increase in
370 the time-temperature roasting profile. This will reduce both batch inhomogeneity, and potentially
371 energy consumption, provided the necessary changes to maintain similar time-temperature
372 profiles are minimal.

373 To increase bean-to-bean conductive heat transfer rates (similar to those in drum roasters),
374 process conditions that employ a large bean bed area with little bed fluidisation are needed; to
375 improve air-to-bean convective heat transfer, as well as convection through bean bed voids, air
376 flow should be maximised to maintain a large fraction of beans in the freeboard – this method is
377 recommended to improve batch consistency.

378 4.3 Impact on temperature measurement

379 The complexity of the flow pattern will affect the measured temperature, depending on where that
380 temperature was measured. Thermocouples in the bean bed will measure a combination of bean

381 and air temperature. At the start of roasting the temperature of the air in the roasting chamber will
382 be higher than in the beans but, as the roast progresses, bean temperature will approach that of
383 the air. As the packing density around the thermocouple will be affected by the local flow
384 behaviour, heat transfer from the bean bed environment to the thermocouple will be affected. It is
385 expected that as the packing density decreases during roasting (i.e., the bed expands and
386 becomes more fluidised) there would be increased contact area between the thermocouple and
387 the air, and a decreased contact area between the thermocouple and beans. The measured
388 'bean' temperature will thus be overestimated, as the air temperature is greater than the beans.
389 This problem adds complexity to comparing time-temperature profiles for dissimilar roasting
390 conditions.

391 4.4 Comparison with previous studies

392 There are some models for roaster behaviour. Single-bean CFD simulations (Chiang et al., 2017)
393 – considering convective heat transfer only – suggested that the uniformity of in-bean temperature
394 distributions increases during the first 1 min 10 s (100 s) of roasting. The impact of bean volume
395 on the temperature and moisture distributions (Abdul Ghani et al., 2019) endorsed adjustment of
396 time-temperature roasting profiles according to the size of green coffee beans. In each of these
397 studies, changes in bean volume during roasting were not considered. The PEPT measurements
398 – particularly those in Figure 8 – suggest that changes to airflow should be performed according
399 to the volumetric expansion of coffee during roasting. Such changes are expected to promote the
400 uniform development of moisture and colour within the bean – although lower energy input
401 increases process time.

402 For heat and mass transfer simulations, Bustos-Vanegas (2015) implemented subroutines to
403 describe (i) density changes as a function of moisture (ii) volumetric expansion as a function of
404 both moisture and applied air temperature during roasting. Although the estimated global heat
405 transfer coefficients were discussed and validated (Bustos-Vanegas 2015), PEPT measurements

406 – particularly those in Figure 8 – suggest that for a system with constant airflow, as bean density
407 decreases a greater number will be propelled into the *dilute* freeboard, where convective heat
408 transfer is dominant – the global heat transfer coefficient would increase as roasting proceeds.

409 CFD-DEM studies of grain drying (Azmir et al., 2020) observed convection-dominant drying at
410 high air velocities in a fluidised bed, with conductive heat transfer increasing as airflow decreases.
411 DEM simulations of coffee roasting in fluidised beds (Bruchmüller et al., 2010) suggest that the
412 global heat transfer coefficient is greatest during the intermittent lifting of beans into the freeboard,
413 resulting in periodic variation of the heat transfer coefficient during roasting. The PEPT
414 measurements shown here also suggest differences in heat transfer in the spouted bed roaster.
415 Differences in the rate of convective heat transfer in the bed and freeboard will create periodic
416 variations of the single-bean heat transfer coefficient due to cyclic particle motion. The next stages
417 of work will be to develop a roasting model using the PEPT data as a basis.

418 **5 Conclusions**

419 PEPT has been used to capture particle dynamics of coffee beans inside a spouted bed roaster
420 at ambient temperatures. Coffees of different roast degrees and densities were studied to emulate
421 the effects of roasting, while the batch size and air mass flow rate were varied to study the impact
422 of air-to-bean ratio on particle dynamics.

423 PEPT data was used to identify the location and subsequent trajectories of a single bean with
424 time. Through calculation of fractional residence times, occupancy of the roasting chamber
425 revealed two different regions: a *dense* bean bed and a *dilute* freeboard. The effect of changing
426 air flow, batch size and bean density has been demonstrated. Beans become less dense and the
427 flow pattern changes as roasting proceeds, which changes the heat transfer characteristic of the
428 roaster in both regions (i.e., bean bed and freeboard).

429 The potential to optimise heat transfer during roasting (i.e., increase efficiency) has been
430 discussed. Overall, this work demonstrates that PEPT can be a useful tool to understand granular
431 flow patterns in roasters. The identified evolution of regional mass fractions and corresponding
432 residence times provide quality data (i.e., dynamic boundary conditions) to be used to improve
433 heat and mass transfer models for roasting.

434 **Acknowledgements**

435 Authors acknowledge funding received from EPSRC through the Centre for Doctoral Training in
436 Formulation Engineering (grant no. EP/L015153/1), and from Jacobs Douwe Egberts.

437 **Author statement**

438 Mark Al-Shemmeri: Investigation, Experimental work and analysis, Writing – original draft; Kit
439 Windows-Yule: Experimental work and analysis, Writing – review & editing; Estefania Lopez-
440 Quiroga: Formal analysis, Supervision, Writing – review & editing; Peter Fryer: Conceptualization,
441 Writing – review & editing, Supervision, Funding acquisition.

442 **Declaration of competing interests**

443 Mark Al-Shemmeri is in receipt of an EngD studentship grant supported by Jacobs Douwe Egberts
444 and EPSRC.

445 **References**

446 Abdul Ghani, N.H., Bingol, G., Li, B., Yu, W., Young, B., (2019). Development of a novel 2D single
447 coffee bean model and comparison with a 3D model under varying heating profiles. *Journal of*
448 *Food Process Engineering* 42(4). <https://doi.org/10.1111/jfpe.13063>

449 Alessandrini, L., Romani, S., Pinnavaia, G., Rosa, M.D., (2008). Near infrared spectroscopy: An
450 analytical tool to predict coffee roasting degree. *Analytica Chimica Acta* 625(1), 95-102.
451 <https://doi.org/10.1016/j.aca.2008.07.013>

452 Alonso-Torres, B., Hernández-Pérez, J.A., Sierra-Espinoza, F., Schenker, S., Yeretjian, C.,
453 (2013). Modeling and Validation of Heat and Mass Transfer in Individual Coffee Beans during the
454 Coffee Roasting Process Using Computational Fluid Dynamics (CFD). *Chimia* 67(4), 291-294.
455 <https://doi.org/10.2533/chimia.2013.291>

456 Azmir, J., Hou, Q., Yu, A., (2020). CFD-DEM study of the effects of food grain properties on drying
457 and shrinkage in a fluidised bed. *Powder Technology* 360, 33-42.
458 <https://doi.org/10.1016/j.powtec.2019.10.021>

459 Baggenstoss, J., Poisson, L., Kaegi, R., Perren, R., Escher, F., (2008). Coffee Roasting and
460 Aroma Formation: Application of Different Time–Temperature Conditions. *Journal of agricultural*
461 *and food chemistry* 56(14), 5836-5846. <https://doi.org/10.1021/jf800327j>

462 Bergman, T.L., DeWitt, D.P., Incropera, F., Lavine, A.S., (2011). *Fundamentals of Heat and Mass*
463 *Transfer*. 9780470501979.

464 Brown, S.L., Lattimer, B.Y., (2013). Transient gas-to-particle heat transfer measurements in a
465 spouted bed. *Experimental Thermal and Fluid Science* 44, 883-892.
466 <https://doi.org/10.1016/j.expthermflusci.2012.10.004>

467 Bruchmüller, J., Gu, S., Luo, K., Van Wachem, B., (2010). Discrete element method for multiscale
468 modeling. *Journal of Multiscale Modelling* 2(01n02), 147-162.
469 <https://doi.org/10.1142/S1756973710000254>

470 Bustos-Vanegas, J. (2015) Modelagem das propriedades físicas e da transferência de calor e
471 massa dos grãos de café durante a torrefação. Master's thesis. Federal University of Viçosa.
472 <https://locus.ufv.br//handle/123456789/7350>

473 Bustos-Vanegas, J., Correa, P., Martins, M., Baptestini, F., Campos, R., Horta de Oliveira, G.,
474 Nunes, E., (2018). Developing predictive models for determining physical properties of coffee
475 beans during the roasting process. *Industrial Crops and Products* 112, 839-845.
476 <https://doi.org/10.1016/j.indcrop.2017.12.015>

477 Cheng, G., Gan, J., Xu, D., Yu, A., (2020). Evaluation of effective thermal conductivity in random
478 packed bed: Heat transfer through fluid voids and effect of packing structure. *Powder Technology*
479 361, 326-336. <https://doi.org/10.1016/j.powtec.2019.07.106>

480 Chiang, C.-C., Wu, D.-Y., Kang, D.-Y., (2017). Detailed Simulation of Fluid Dynamics and Heat
481 Transfer in Coffee Bean Roaster. *Journal of Food Process Engineering* 40(2), e12398.
482 <https://doi.org/10.1111/jfpe.12398>

483 Cristo, H.P., Martins, M.A., Oliveira, L.S., Franca, A.S., (2006). Transverse flow of coffee beans
484 in rotating roasters. *Journal of Food Engineering* 75(1), 142-148.
485 <https://doi.org/10.1016/j.jfoodeng.2005.04.010>

486 Díaz-Heras, M., Belmonte, J.F., Almendros-Ibáñez, J.A., (2020). Effective thermal conductivities
487 in packed beds: Review of correlations and its influence on system performance. *Applied Thermal*
488 *Engineering* 171, 115048. <https://doi.org/10.1016/j.applthermaleng.2020.115048>

489 Garcia, C. D. C., Pereira Netto, A. D., Silva, M. C. D., Catão, A. A., Souza, I. A. D., Farias, L. S.,
490 ... & Silva Junior, A. I. D. (2018). Relative importance and interaction of roasting variables in coffee
491 roasting process. *Coffee Science* – 13(3), 379-388. <http://dx.doi.org/10.25186/cs.v13i3.1483>

492 Geiger, R., Perren, R., Kuenzli, R., Escher, F., (2005). Carbon Dioxide Evolution and Moisture
493 Evaporation During Roasting of Coffee Beans. *Journal of Food Science* 70(2), E130.
494 <https://doi.org/10.1111/j.1365-2621.2005.tb07084.x>

495 Hoos, R., (2015). *Modulating the Flavour Profile of Coffee*. Lulu Press, Inc. ISBN-10 :
496 0692417702.

497 Kwak, H.S., Ji, S., Jeong, Y., (2017). The effect of air flow in coffee roasting for antioxidant activity
498 and total polyphenol content. *Food Control* 71, 210-216.
499 <https://doi.org/10.1016/j.foodcont.2016.06.047>

500 Oliveros, N.O., Hernández, J.A., Sierra-Espinosa, F.Z., Guardián-Tapia, R., Pliego-Solórzano, R.,
501 (2017). Experimental study of dynamic porosity and its effects on simulation of the coffee beans
502 roasting. *Journal of Food Engineering* 199, 100-112.
503 <https://doi.org/10.1016/j.jfoodeng.2016.12.012>

504 Otsu, N., (1979). A Threshold Selection Method from Gray-Level Histograms. *IEEE Transactions*
505 *on Systems, Man, and Cybernetics* 9(1), 62-66. <https://doi.org/10.1109/TSMC.1979.4310076>

506 Parker, D., Broadbent, C., Fowles, P., Hawkesworth, M., McNeil, P., (1993). Positron emission
507 particle tracking-a technique for studying flow within engineering equipment. *Nuclear Instruments*
508 *and Methods in Physics Research Section A: Accelerators, Spectrometers, Detectors and*
509 *Associated Equipment* 326(3), 592-607. [https://doi.org/10.1016/0168-9002\(93\)90864-E](https://doi.org/10.1016/0168-9002(93)90864-E)

510 Parker, D.J., (2017). Positron emission particle tracking and its application to granular media.
511 Review of Scientific Instruments 88(5). <https://doi.org/10.1063/1.4983046>

512 Parker, D.J., Forster, R.N., Fowles, P., Takhar, P.S., (2002). Positron emission particle tracking
513 using the new Birmingham positron camera. Nuclear Instruments and Methods in Physics
514 Research Section A: Accelerators, Spectrometers, Detectors and Associated Equipment 477(1),
515 540-545. [https://doi.org/10.1016/S0168-9002\(01\)01919-2](https://doi.org/10.1016/S0168-9002(01)01919-2)

516 Pittia, P., Sacchetti, G., Mancini, L., Voltolini, M., Sodini, N., Tromba, G., Zanini, F., (2011).
517 Evaluation of Microstructural Properties of Coffee Beans by Synchrotron X-Ray
518 Microtomography: A Methodological Approach. Journal of Food Science 76(2), E231.
519 <https://doi.org/10.1111/j.1750-3841.2010.02009.x>

520 Rao, S., (2014). *The Coffee Roaster's Companion*. ISBN-10 : 1495118193.

521 Rao, S., (2020). *Coffee Roasting - Best Practices*. ISBN-10 : 1792327757.

522 Resende, I.A., Machado, M.V.C., Duarte, C.R., Barrozo, M.A.S., (2017). An experimental analysis
523 of coffee beans dynamics in a rotary drum. The Canadian Journal of Chemical Engineering
524 95(12), 2239-2248. <https://doi.org/10.1002/cjce.22961>

525 Romani, S., Cevoli, C., Fabbri, A., Alessandrini, L., Dalla Rosa, M., (2012). Evaluation of Coffee
526 Roasting Degree by Using Electronic Nose and Artificial Neural Network for Off-line Quality
527 Control. Journal of Food Science 77(9), C965. <https://doi.org/10.1111/j.1750-3841.2012.02851.x>

528 Schenker, S., (2000). Investigations on the hot air roasting of coffee beans. ETH Zürich.
529 <https://doi.org/10.3929/ethz-a-003889071>

530 Schwartzberg, H. (2002) Modeling Bean Heating during Batch Roasting of Coffee Beans. In
531 Welte-Chanes, J., Barbosa-Canovas, G., Aguilera, MJ., editors. Engineering and food for the
532 21st century, Boca Raton: CRC Press LLC. <https://doi.org/10.1201/9781420010169>

533 Wang, N., Lim, L.-T., (2012). Fourier Transform Infrared and Physicochemical Analyses of
534 Roasted Coffee. *Journal of agricultural and food chemistry* 60(21), 5446-5453.
535 <https://doi.org/10.1021/jf300348e>

536 Wildman, R.D., Huntley, J.M., Hansen, J.P., Parker, D.J., Allen, D.A., (2000). Single-particle
537 motion in three-dimensional vibrofluidized granular beds. *Physical review. E, Statistical physics,*
538 *plasmas, fluids, and related interdisciplinary topics* 62(3 Pt B), 3826-3835.
539 <https://doi.org/10.1103/physreve.62.3826>

540 Wilson, P.S., (2014). Coffee roasting acoustics. *The Journal of the Acoustical Society of America*
541 135(6), EL269. <https://doi.org/10.1121/1.4874355>

542 Windows-Yule, C., Seville, J., Ingram, A., Parker, D., (2020). Positron Emission Particle Tracking
543 of Granular Flows. *Annual review of chemical and biomolecular engineering.*
544 <https://doi.org/10.1146/annurev-chembioeng-011620-120633>

545 Yergenson, N., Aston, D.E., (2020). Monitoring coffee roasting cracks and predicting with in situ
546 near-infrared spectroscopy. *Journal of Food Process Engineering* 43(2), e13305.
547 <https://doi.org/10.1111/jfpe.13305>

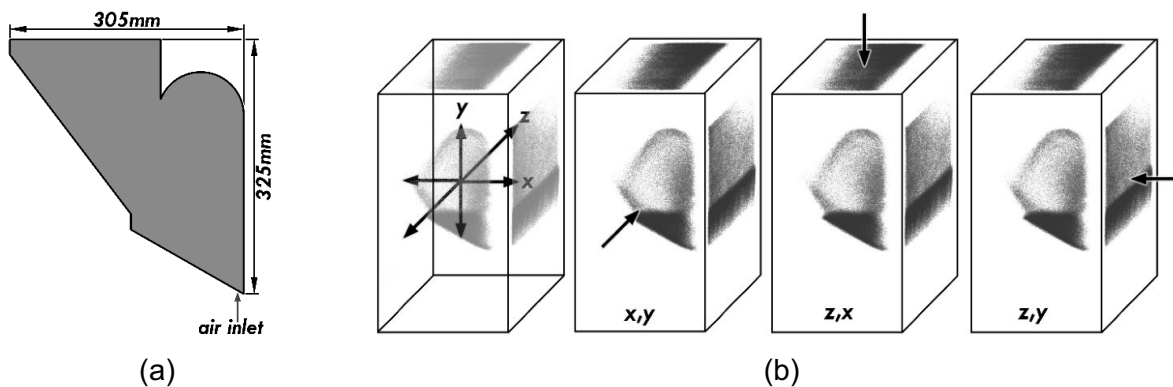


Figure 1. Description of roasting system, outlining (a) a simplified schematic of the spouted bed roasting chamber and (b) established orientation of system volume using a simplified, cubic schematic of the roaster overlaid with recorded tracer positions from a single run (200g of part-roasted coffee beans at a fan frequency of 48 Hz).

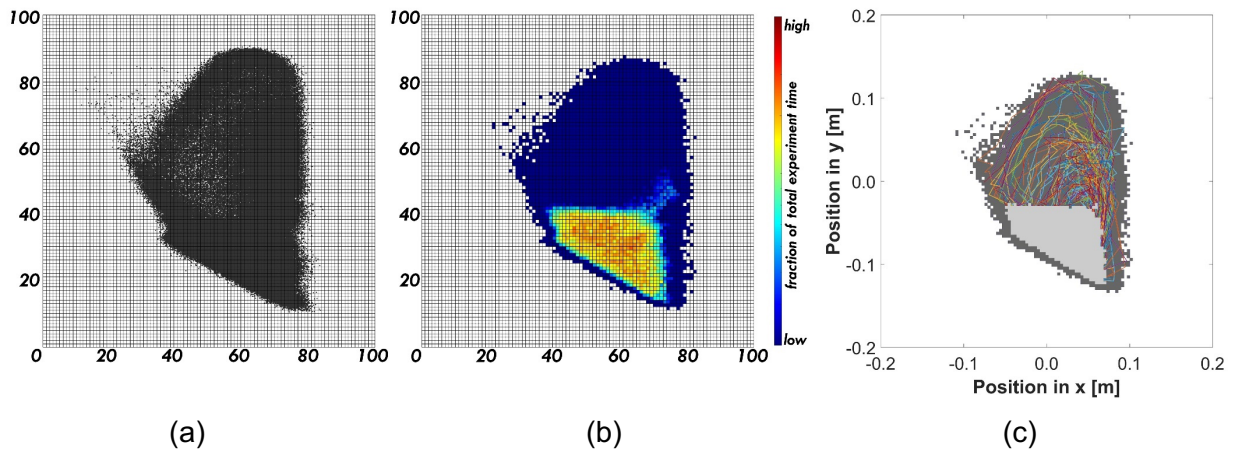


Figure 2. Subdivided system volume of 100x100 elements of 3.5x3.5 mm - in plane xy - overlaid with (a) all experimental data points and (b) the occupancy profile of an individual run, from which (c) an example of individual particle trajectories (multi-colour) - tracked from the spout, through the freeboard (dark grey) until their return to the bean bed (light grey) - can be identified. Data displayed in (b) and (c) relates to a 200g batch of part-roasted coffee beans where the roaster fan frequency was set to 48Hz.

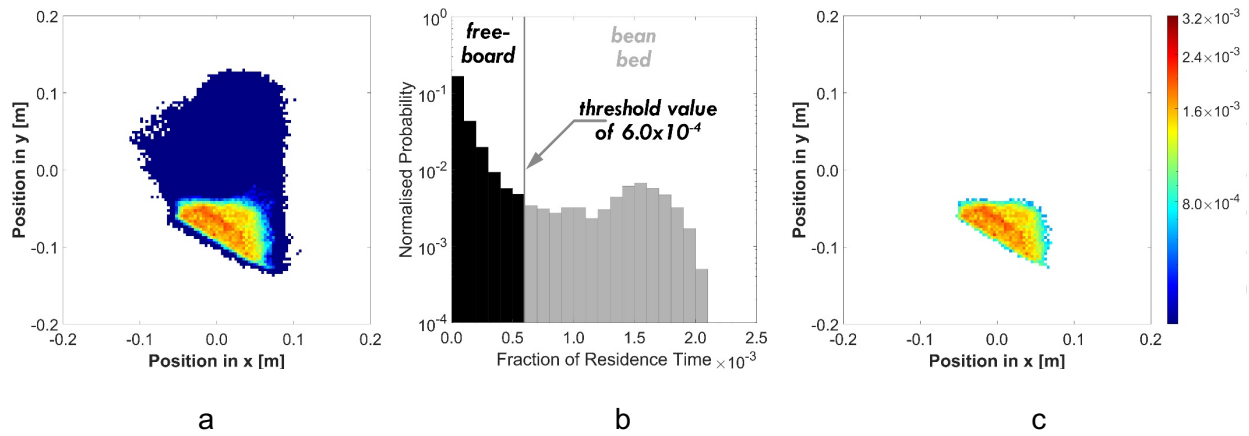


Figure 3. Visualisation of the Otsu method thresholding process to delineate a) total occupancy via determination of a threshold value based on b) normalised probability distributions of fractional residence time in y to reveal c) bed occupancy.

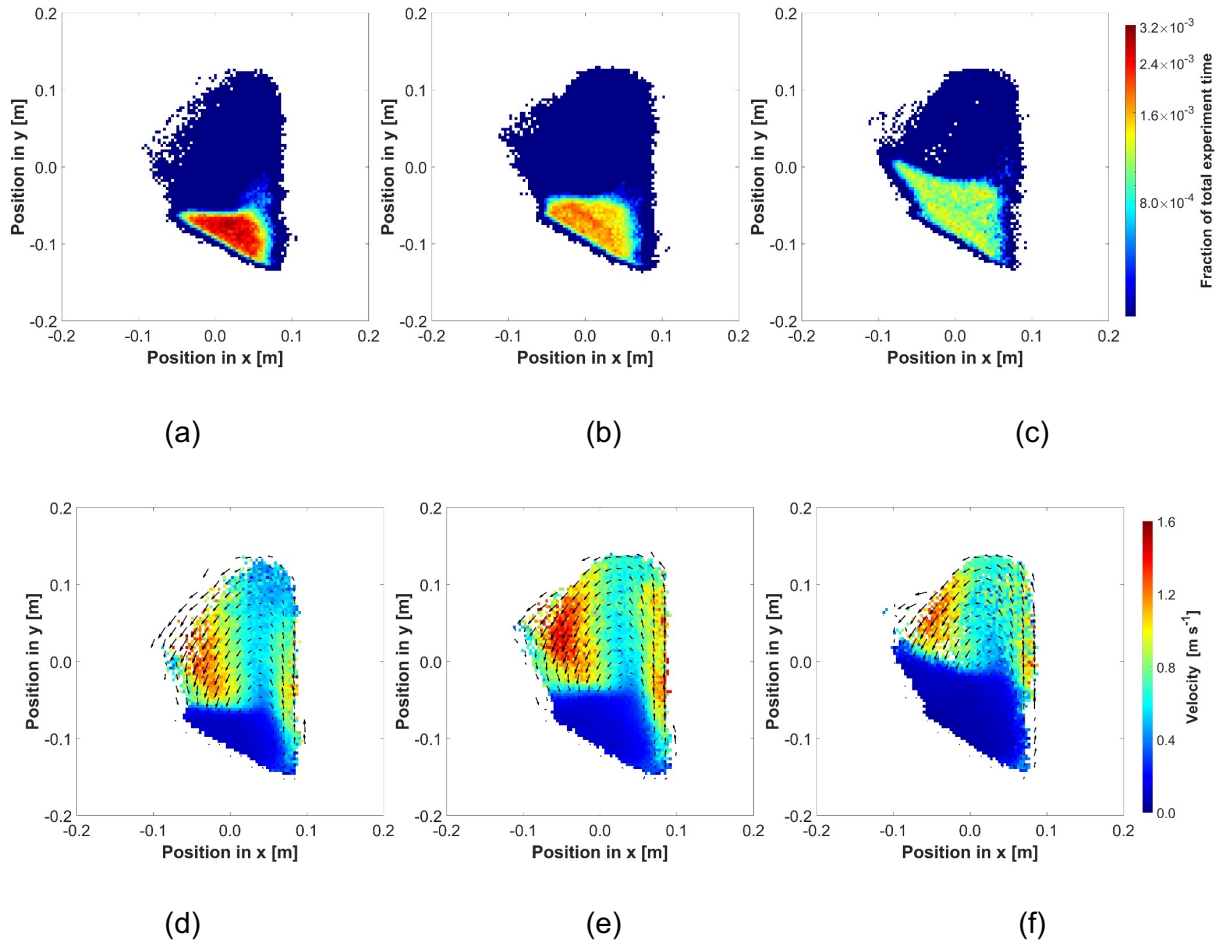


Figure 4. Comparison of (a)-(c) occupancy and (d)-(f) velocity (in plane xy) profiles obtained from PEPT data corresponding to batches of 350g of coffee of different density studied at a fan frequency of 48 Hz. Coffee bean densities correspond to: (a) and (d), green; (b) and (e), part-roasted; (c) and (f), roasted coffee.

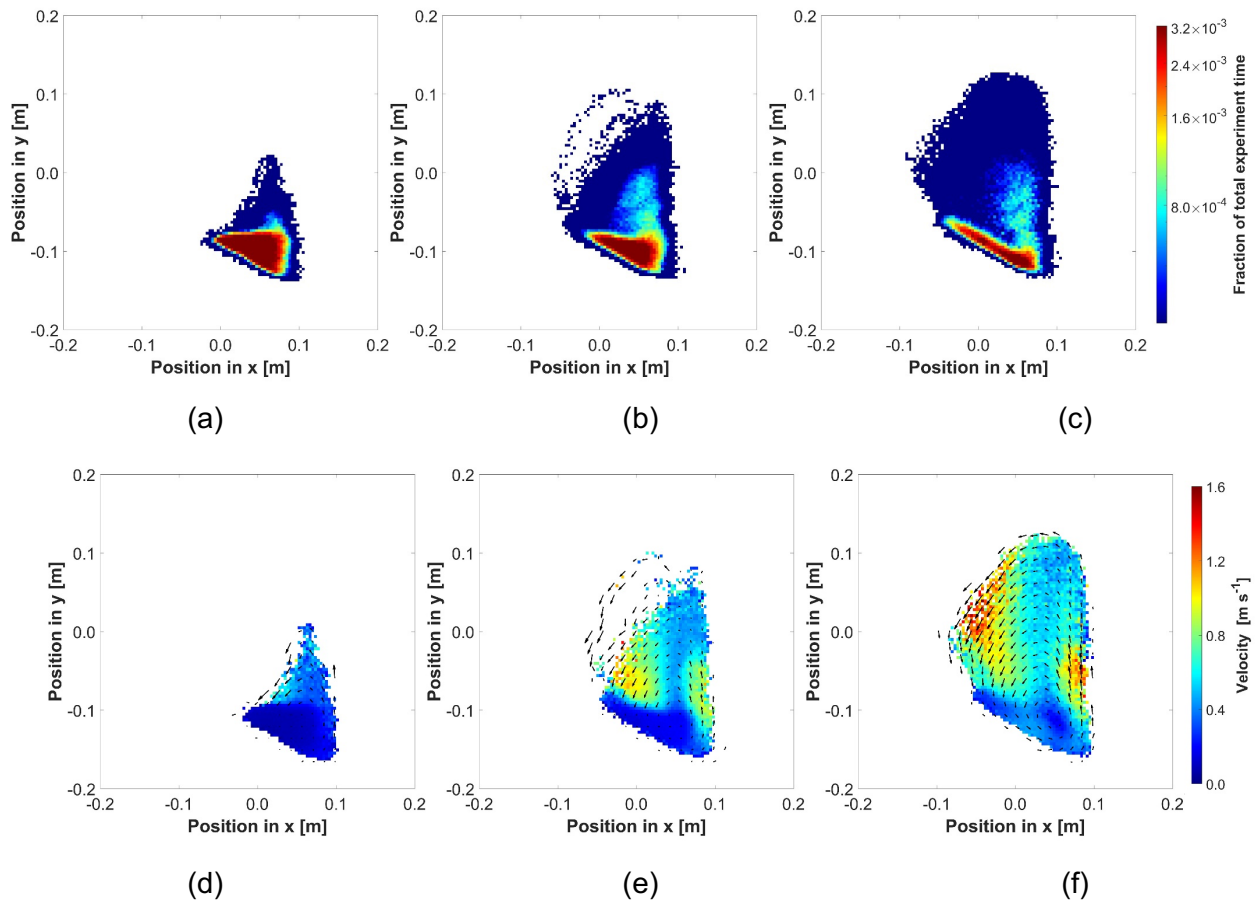


Figure 5. Comparison of (a)-(c) occupancy and (d)-f) velocity (in plane xy) profiles for 200g batches of green coffee subject to different airflows. Airflows correspond to fan frequencies of: (a) and (d), 30 Hz; (b) and (e), 48 Hz; (c) and (f), 65 Hz.

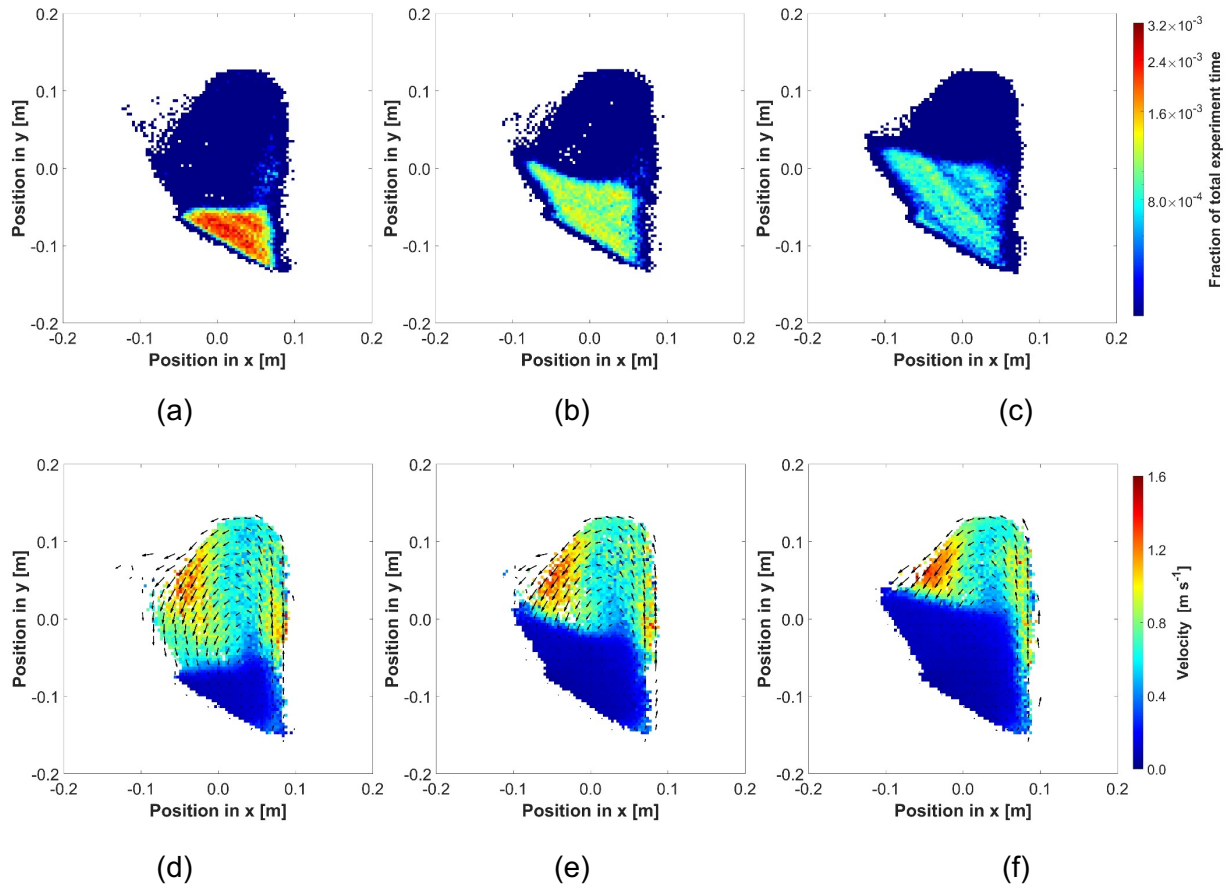


Figure 6. Comparison of (a)-(c) occupancy and (d)-(f) velocity (in plane xy) profiles for roasted coffee of different batch sizes subject to air at a fan frequency of 48 Hz. Batch sizes correspond to: (a) and (d), 200g; (b) and (e), 350g; (c) and (f), 500g.

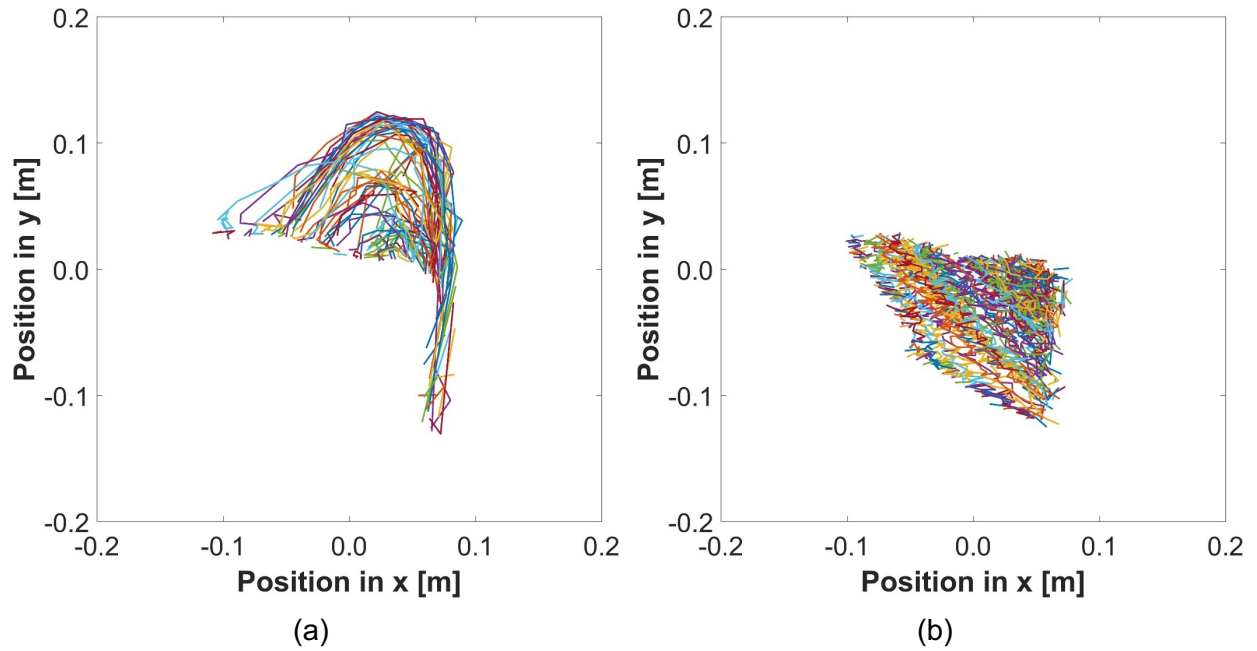


Figure 7. Particle trajectories of a coffee bean within the a) freeboard and b) bed obtained from PEPT data corresponding to a batch of 500g of roasted coffee subject to moderate airflow (48 Hz). Data is the same as that plotted in Figures 6 (c) and 6 (f).

555

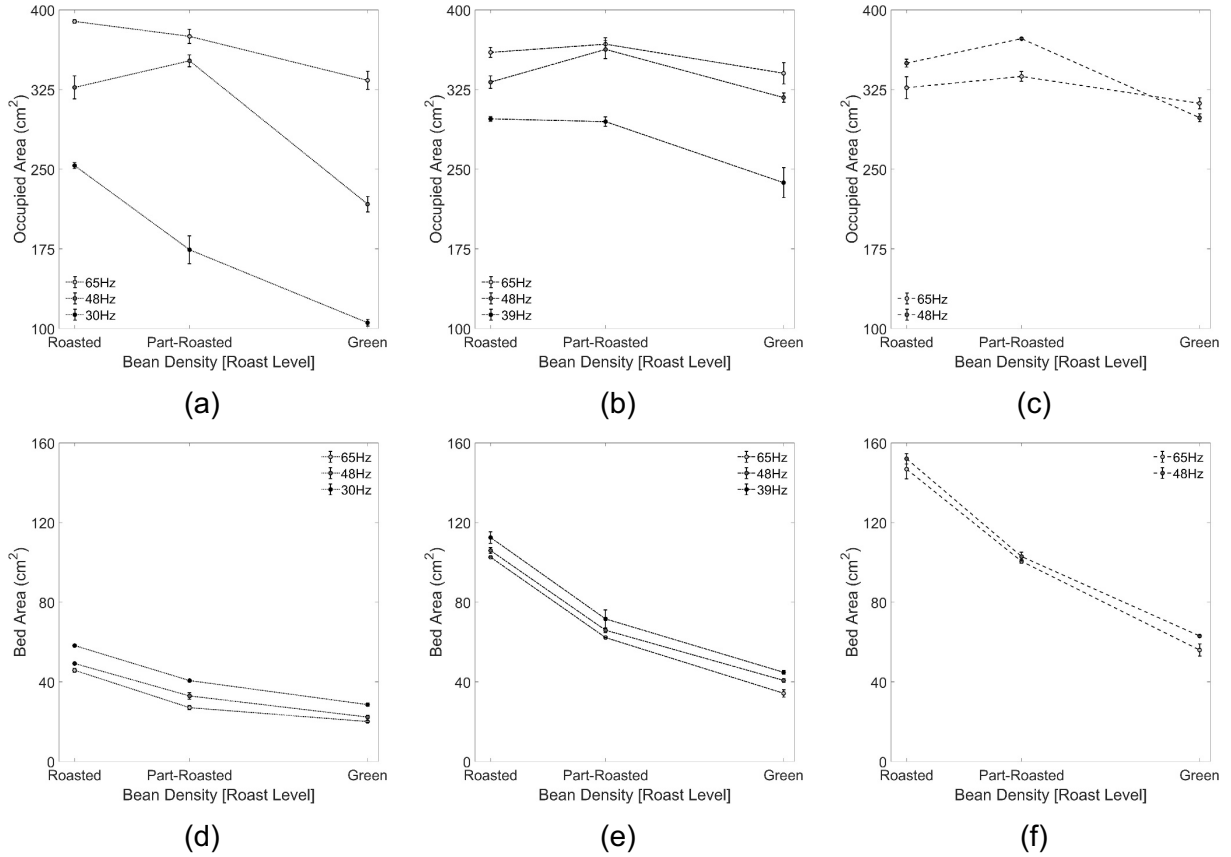


Figure 8. Changes in (a)-(c) occupied area and (d)-(f) bed area as a function of coffee density and airflow for batch sizes of: (a) and (d) 200g; (b) and (e) 350g and (e) and (f) 500g, in plane xy.

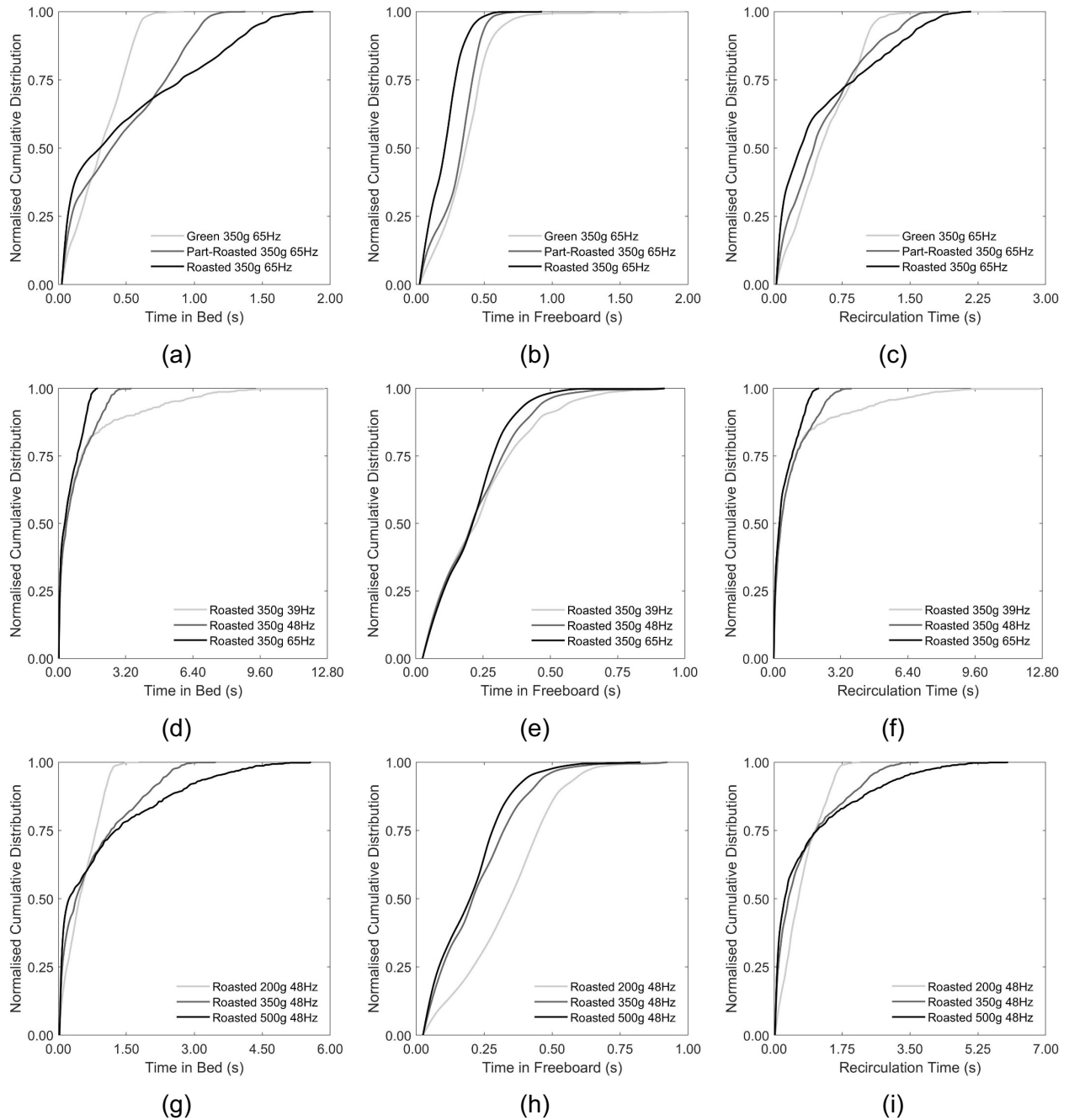


Figure 9. Cumulative distributions of residence time (a), (d) and (g) in the bed, (b), (e) (h) in the freeboard and (c), (f) and (i) from spout-to-spout (i.e., recirculation times, where spout-to-spout residence times are the sum of the freeboard and bed residence times). The effect of coffee density is shown in (a)-(c) for 350g of coffee with different densities subject to high (65 Hz) airflow; the effect of air flow is shown in (d)-(f) for 350g of roasted coffee subject to different air flows; the effect of batch size is shown in (g)-(i) for different batch sizes of roasted coffee at moderate (48 Hz) airflow.

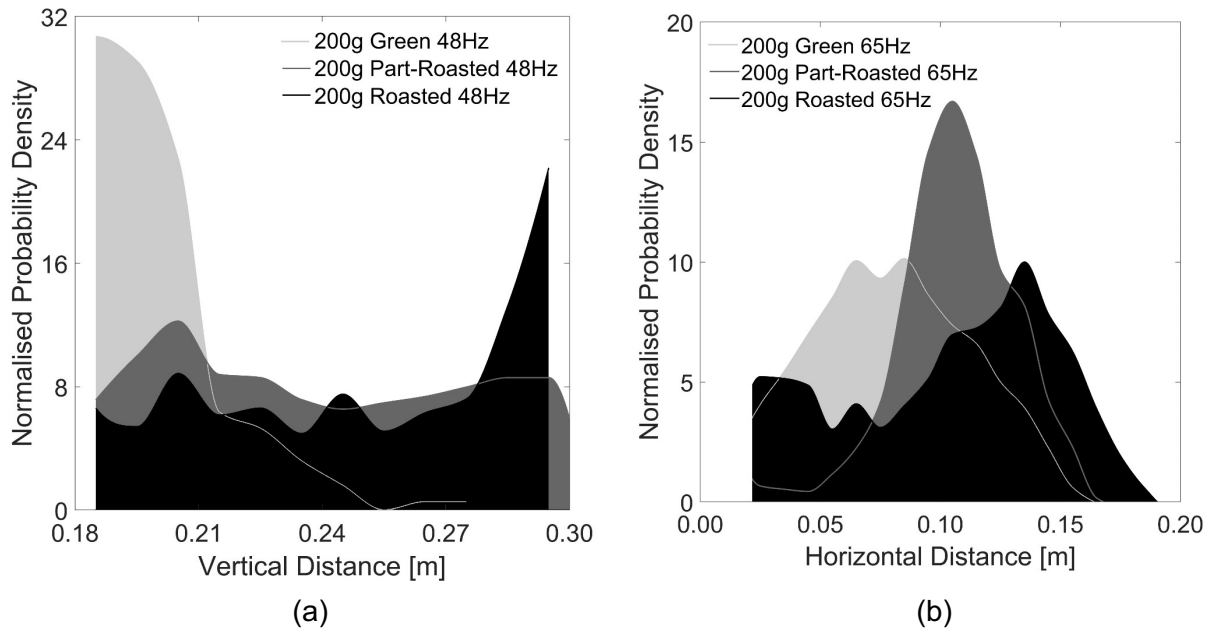


Figure 10. Changes in (a) vertical and (b) horizontal freeboard distances traversed by coffees beans of different densities in a 200g batch at a) moderate (48Hz) and b) high (65Hz) air flow.

Table 1. Properties of Kenyan Arabica coffee beans of different roasting degrees.

Coffee Sample	Roast Time (s)	Roast Loss (%)	Principal Dimension a (mm)	Principal Dimension b (mm)	Principal Dimension c (mm)	Volume (mm ³)	Intrinsic Density (kg m ⁻³)	Bulk Density (kg m ⁻³)
Green	0	0.0	6.18±0.34	3.84±0.41	8.54±0.62	106±3	1311±12	705±11
Part-Roasted	138	8.1	7.08±0.50	4.42±0.48	9.07±0.83	151±7	844±23	460±9
Roasted	278	16.6	7.64±0.49	4.80±0.44	10.38±0.86	206±5	589±8	301±6

Table 2. Airflow properties of the spouted bed roaster as determined by a hot-wire anemometer.

Fan Frequency (Hz)	Air Velocity (m s⁻¹)	Air Mass Flow Rate (kg s⁻¹)
30	4.2	0.0141
39	5.7	0.0185
48	7.2	0.0228
65	10.0	0.0310

561

Table 3. Static bean bed area of coffee beans as affected by batch size and bean density in plane *xy*.

Batch Size (g)	Coffee Sample	Bed Area in <i>xy</i> (cm²)
200	Green	28.85±0.42
	Part-Roasted	44.25±0.87
	Roasted	83.44±2.55
350	Green	50.50±0.76
	Part-Roasted	103.28±3.03
	Roasted	184.71±4.47
500	Green	92.67±2.16
	Part-Roasted	169.65±4.33
	Roasted	285.99±6.39

562